Understanding the Aerodynamics of a Paper Plane

Shaik Sajeed HUSSAIN , Ramit RAKESH, and Phani Raghava PANCHAGNULA
Institut Supérieur de l'Aéronautique et de l'Espace, Toulouse, France, 31400

I. Introduction

Understanding the performance of a paper plane involves delving into various aspects of its design and aerodynamics. Aerodynamics and paper folding quality plays a crucial role in determining how well a paper plane flies, and conducting flow analysis on its wings can provide valuable insights. Essentially exploring factors such as wing shape, sweep angle, aspect ratio, angle of attack, and even the presence of features like a ventral gap can significantly impact the plane's flight characteristics. The dynamics of the paper plane are equally important because there is only initial thrust and no active controllers.

The objective of this project is to analyze the flow structure, in particular vortex-formation and the effect of ventral gap of the Suzanne and design a paper-plane with an A4 sheet to improve range and performance. The intended mission profile is illustrated in the Fig. 1 and the corresponding requirement in Table 1.

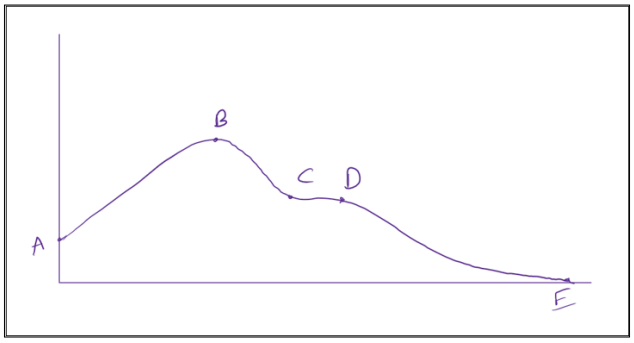

Fig. 1 Mission Profile

Table 1 Mission Requirements

	Mission Phase	Requirement
A - B	Climb	Slender design and no moment
B - C	Stall and dive	Create pitch up moment
C - D	Recovery	Maintain short level flight
D - E	Glide	Higher AR design

II. Models

In this study we have compared 4 paper airplane models, all with their unique characteristics to help us better understand the aerodynamics that affect and govern the flow around them and if there is something we could do to improve it.

The first Model as shown in Fig. 2 which has been chosen as a baseline as experimental results [6] are available for that configuration and can use those results to validate CFD results, hence acting as a robust point of comparison to all the other models.

Suzanne[3], as depicted in Fig. 3, was selected as the second model due to its previous status as a world record holder (albeit with different dimensions than the world record holder plane), making it an evident choice for this study. But interestingly what we observed during experimental tests was that the Suzanne would glide very well at lower velocities but in order to increase the range when we throw it much faster it just opens up, i.e the ventral gap (V shaped gap between the paper airplane due to folding) widens. We ended up with more questions than answers, and in particular the effects of the ventral gap puzzled us given the lack of research on this topic. Knowing that rules of the competition we would be constrained to an A4 sheet of paper and nothing else, hence we would not be able to tape the ventral gap in reality but having to understand the influence of the ventral gap on the flow would be beneficial to our cause.

Hence, Suzanne with No Ventral Gap Fig. 4 was chosen also as the 3rd model to simulate a configuration without ventral gap.

Lastly, based on the understandings from the previous 2 configurations after testing we came to design Dart Model Fig. 5. In essence it captures the best of both worlds having a covered Ventral Gap for 0.4 z/c and having a shallow ventral after to use the beneficiary effects on the Ventral Gap to our cause.

Fig. 2 Baseline

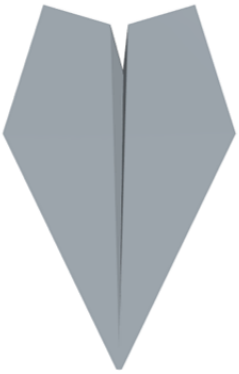

Fig. 3 Suzanne with Ventral Gap

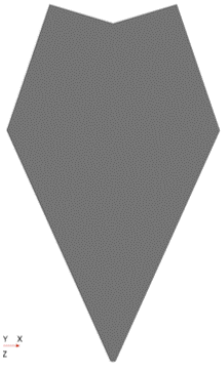

Fig. 4 Suzanne with No Ventral Gap

Fig. 5 Dart

Table 2 Sweep Angles and Aspect Ratios for the different Models

	Baseline	Suzanne Ventral Open	Suzanne Ventral Closed	Dart
Sweep Angle	75°	64.442°	66.942°	82.30°
Aspect Ratio	1.0717	1.913	1.702	0.5408

III. Polhamus's Theory and Code

Polhamus's Theory [5] suggests that the lift from vortex formation can be predicted by modifying potential-flow theory to account for nonlinearities and the loss of lift due to leading-edge suction, offering a more accurate prediction of total lift across a range of angles of attack up to 20° or more.

$$C_L = K_p \sin\alpha \cos^2\alpha + K_v \cos\alpha \sin^2\alpha \tag{1}$$

Eqn.1 is the relation derived by Polhamus to find Lift, and it depends on α, K_p and K_v which in turn depend on Aspect Ratio. The K_p and K_v values need to be found out via their respective graphs, but since the graphs are dated and hard to read it is difficult to read. Hence, we digitised the graphs with the help of code and for the aspect ratio's we found out the exact K_p and K_v values this way as shown in Fig. 6 and Fig.7. Once we had those we could plot the C_L Vs Angle of Attack (α) plots with the help of the python code in the Appendix and that would extrapolate the exact C_L values for the desired α as shown in Fig.8.

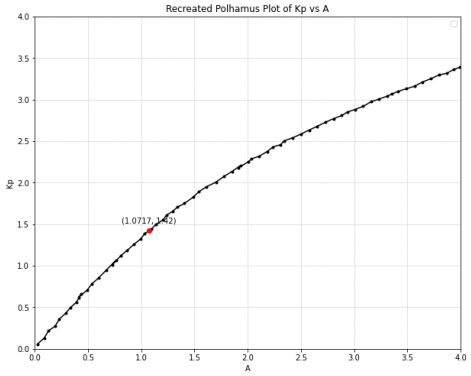

Fig. 6 K_p Plot

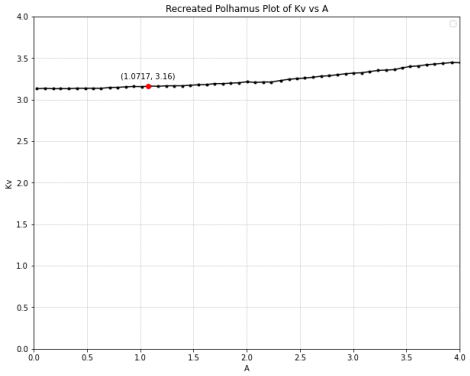

Fig. 7 K_v Plot

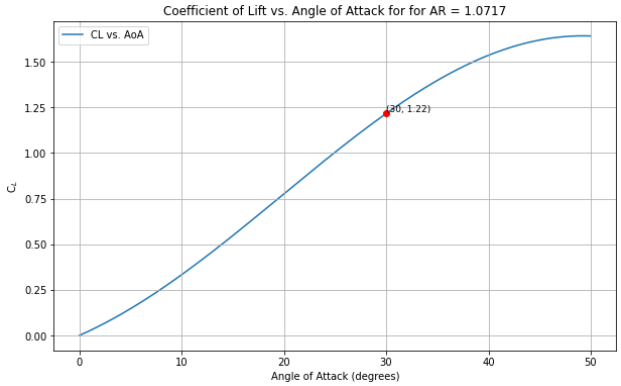

Fig. 8 Polhamus C_L vs α Plot for AR = 1.0717

IV. Numerical Setup and Validation

A. Setup and Mesh

The commercial computational fluid dynamics software STAR_CCM+ was utilized for simulating the airflow around the specified shapes, as illustrated in figures 2 to 5. The flow is three-dimensional, assumed to be incompressible and steady-state. The computational model employed the Reynolds Averaged Navier-Stokes equations using the $k-\omega$ SST Turbulence model. The chord-wise Reynolds number is set at $Re = 75,000$. Despite the relatively low Reynolds number, no transitional flow model was applied, assuming the flow to be entirely turbulent. This omission was made to reduce computational time and expense. The simulation did not account for transient behaviors, thus necessitating a cautious examination of the airflow at higher angles of attack, where stall phenomena are likely. To minimize computational demands, only half of the geometry was simulated, and the aircraft's nose was designed to be slightly blunt rather than sharp to enhance mesh quality. As indicated by Chang et al. [2], the ventral part was also simulated using the Suzanne geometry, as depicted in Fig.3.

Fig.9 shows the boundary conditions for the computational domain. An adiabatic no-slip wall boundary condition is applied to the geometry of the airplane. The plane cutting the geometry in the middle of the geometry is considered a symmetry plane. An unstructured hexahedral mesh was built. The boundaries in the far-field are applied with a surface control to not have the boundary layer mesh on the boundaries- inlet, outlet, and far-field. A prism layer mesher was used around the airplane and a Y^+ of 5 was imposed, giving about 8 prism layers. The Y^+ value is chosen in such a way because the vortex roll-up originates from the sharp leading edge and isn't dependent on the nature of the boundary layer. Therefore the mesh refinement is focused on the resolution of the wing vortex. A mesh refinement is done around the airplane upto a distance of 2 chords from the geometry in all directions. Additionally, the surface control on the far

boundaries also allows to have larger cells (coarse mesh) and more refined mesh closer to the airplane. The refinement is illustrated in Fig/9.

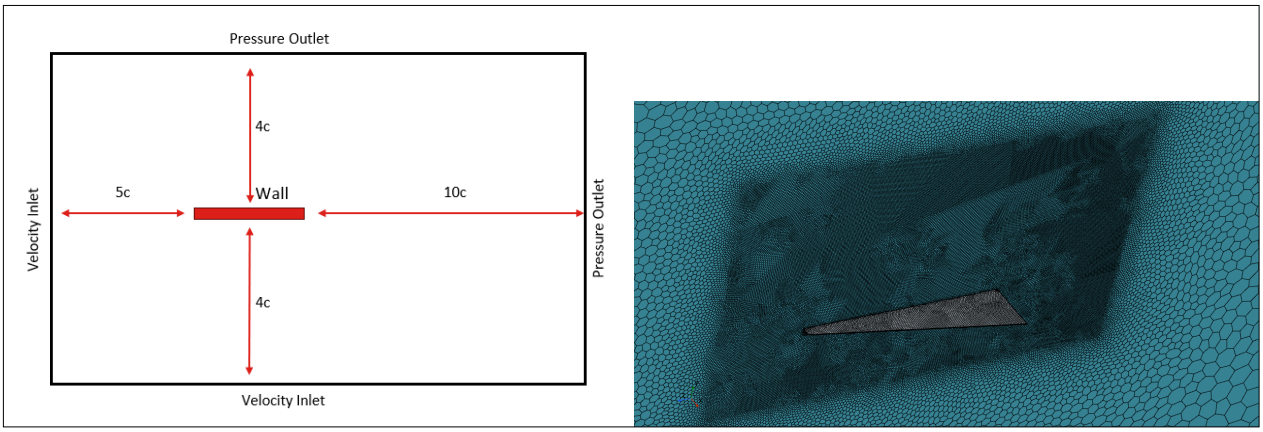

Fig. 9 Boundary Conditions in the CFD setup (Left). Refinement round the plane (Right)

B. Mesh Convergence

A mesh convergence study is conducted using 4 different meshes. The targeted quantities are lift and drag coefficients (C_L and C_D) at 38° angle of attack. The different Mesh size and their %variation in C_L and C_D are shown in table 3. The first mesh was Mesh 3 (M3). Then later three more meshes were prepared(M1, M2, and M3). Finally, the mesh chosen is M2 because the % variation was not that high and M3 and M4 were computationally intensive.

Table 3 Mesh size and percentage variation in CL and CD.

Mesh	No. of Elements	% variation of C_L and C_D
M1	2.3 Million	2.2
M2	2.9 Million	1.61
M3	4 Million	1.10
M4	5 Million	1.10

C. Validation and comparison study

The validation of CFD results is done by comparing with both Polhamus Theory [5] and experimental results provided by Schulter in his paper[6]. The experimental data was obtained with water tunnel testing. Fig.10 illustrated the Lift coefficient(C_L) Vs α for the geometries chosen. The data of CFD is only until 40° angle of attack. The baseline geometry used is from[6]. For the baseline geometry, we can see that the Polhamus and steady RANS results are quite near to the experimental data at low angles of attack. But at higher angles of attack, the theory and CFD start to deviate. This is because the CFD simulations were steady and since at higher AOA where stall occurs, unsteadiness is very important is not being taken into consideration and the prediction of vortex breakdown during stall is not very accurate and cannot be trusted without an unsteady simulation.

The interest was also in the effect of the ventral gap as said by Chang et.al [2]. According to Chang et.al the ventral gap provides a bit higher lift. Which can be seen in Fig. 10. In the current study, the effect of Ventral gap is studied on Suzanne geometry. The Suzanne with Ventral gap has a higher lift than the Vuzanne without the ventral gap. But the geometry with Ventral gap stalls earlier than the one without. But then again there is no CFD data after 40° angle of attack. Therefore, we cannot comment more on the stall characteristics.

When the paper plane is thrown the ventral gap opens for the entire plane. The opening of Ventral gap can only be avoided by using a plastic tape or by changing the folding technique. Since it was not allowed to use the tape, it was decided to opt for a change of the folding technique. A combination of the closed and open gap is chosen as shown in

Fig. 5. Here for about 30 to 40 percent of the plane had no Ventral gap and the rest of the plane had a open Ventral gap. This geometry is called Dart.

Fig. 11 shows the C_L/C_D Vs angle of attack α for all four geometries. At low angles of attack (Until 15°). The baseline geometry had better performance than the other three. The Suzanne without the Ventral gap had better performance than the one without. This might be because of the backflow vortices which may bring negative pressure zones, which causes the pressure-induced drag to be higher. This is further explained in the Flow analysis section below.

By comparing the performance of the Dart plane with Suzanne with Ventral gap we see that the performance is similar for both Dart and Suzanne with Ventral gap (From $\alpha = 20°to30°$). But at $\alpha > 30°$ we see that the dart plane has better performance than the Suzanne with Ventral gap. This implies that the Ventral gap is only beneficial when it is very much further aft of the airplane.

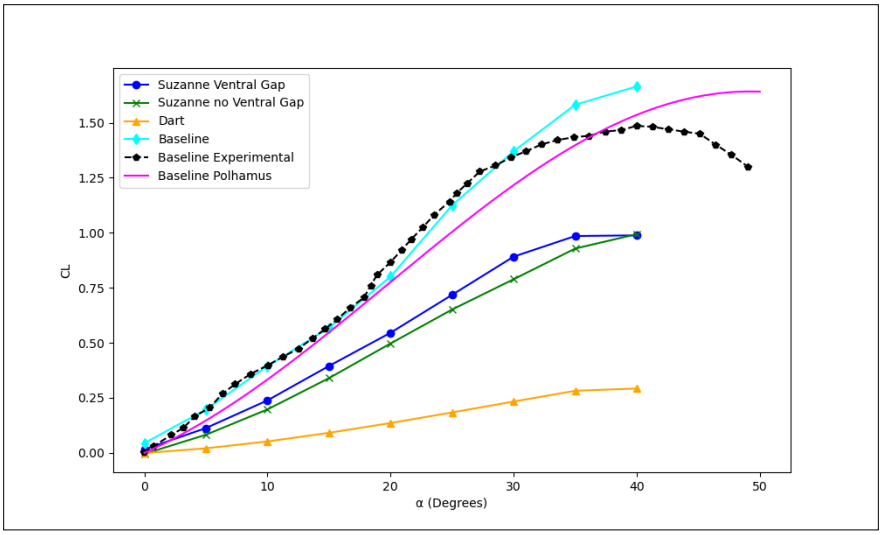

Fig. 10 (Lift Coefficient (C_L) Vs angle of attack α) for different geometries.

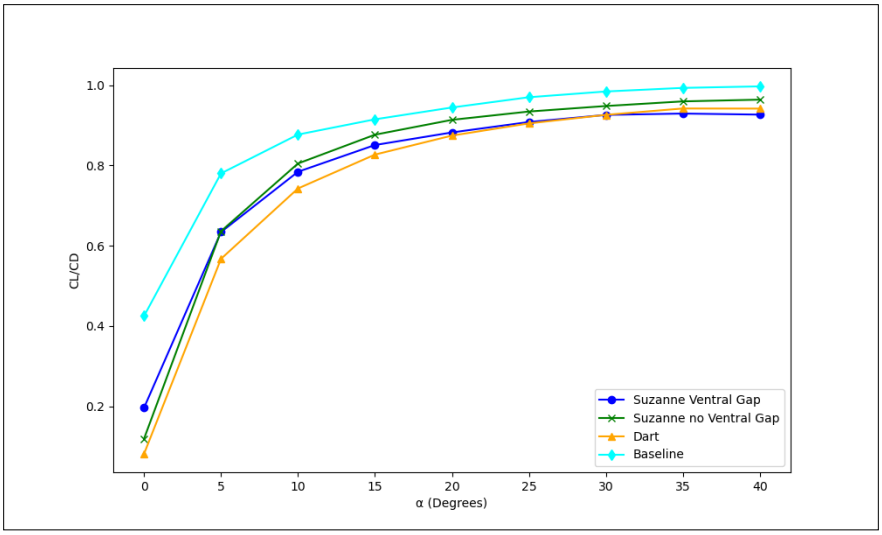

Fig. 11 C_L/C_D Vs angle of attack α for different geometries.

V. Flow Analysis

A. Ventral Gap Closed

Looking at only the upper surface Skin Friction Coefficient Contours Fig.12 at 30° angle of attack, the flow lines are clearly evident and show a trend that is expected and are very familiar with. Initially, it can be seen that the flow is fully attached to the the wing, and as it moves downstream from the inboard and upstream portion of the wing, it can be seen that the flow would turn span-wise in the outboard direction due to the pressure differential near the leading edge, as is depicted in the C_p graph Fig.20 at z/c = 0.37 by the red curve peaks near the leading edge.

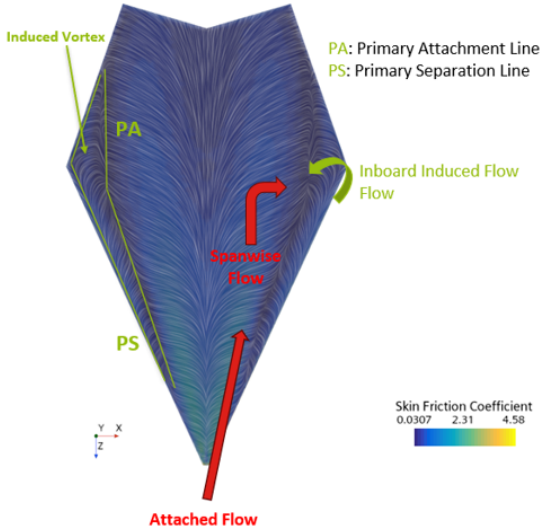

Fig. 12 Skin Friction Coefficient Contours at $\alpha = 30°$ Upper Surface

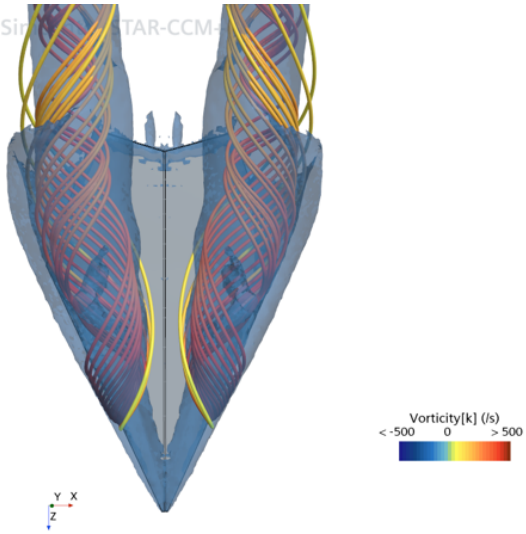

Fig. 13 Iso-contour from Q criterion and Streamlines colored in vorticity at $\alpha = 30°$

In Fig.12 the points of confluence span-wise flow and inboard induced flow over the vortex is the primary attachment line (denoted by PA in the figure) and the point of separation of the vortex from the leading edge is the primary separation line (denoted by PS in the figure). The areas denoting minimal skin friction are due the flow being separated and the presence of the vortex (again confirmed by looking at the Contours in Fig. 13) contributing to the lift as is expected of a sharp delta wing and as has been explained by J.M. Luckring [4].

B. Ventral Gap Open

A quick glance at the Skin Friction Contours in Fig.14 confirms similar flow to Fig. 12 and hence the same analysis could be drawn as has been mentioned in Sub Section V.A with one key difference of course the central area near the Ventral Gap.

This is of course to be expected and in fact what was needed to study and analyse, i.e the key influence of ventral gap presence on flow and its associated aerodynamics. Looking at Fig.14 and concentrating on the region that encompasses the Ventral Gap, it can be seen contrary to Fig.12 the flow tends to curl inboard towards the ventral gap, which again could be explained by the pressure differential near the ventral gap, as has been depicted by Fig.20 with pressure peaks (blue line) observed near the center-line at z/c = 0.89. This of course leads to an additional vortex arising from the ventral gap as has been depicted in the Fig.15, and could be attributed as the reason for us to obtain a higher C_L in the plots.

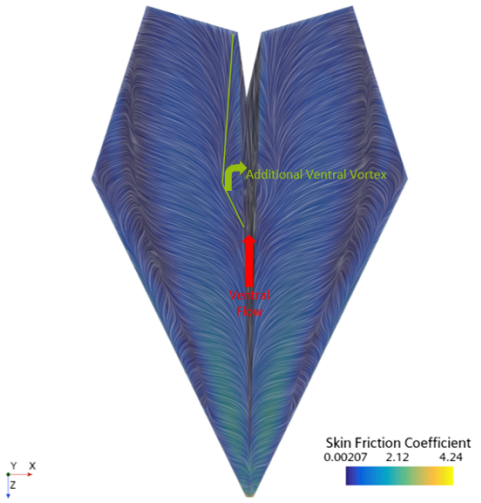

Fig. 14 Skin Friction Coefficient Contours at $\alpha = 30°$ Upper Surface

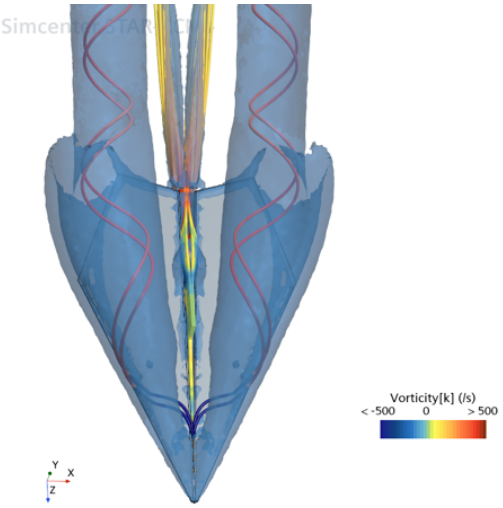

Fig. 15 Iso-contour from Q criterion and Streamlines colored in vorticity at $\alpha = 30°$

VI. Ventral Gap Section

An effort is made to understand the reason why the ventral gap-opened configuration produces more lift than the closed configuration. The Fig:16 shows the spatial vorticity distribution contours of the ventral gap opened configuration at $\alpha = 30°$. The slices are positioned at z/c of 0, 0.26, 0.37, 0.58, 0.68, 0.89, and 0.95 respectively. An interesting phenomenon can be discovered that there is a strong vorticity distribution in the inner part around z/c = 0.58 and onwards, which is absent in the Ventral gap closed configuration.

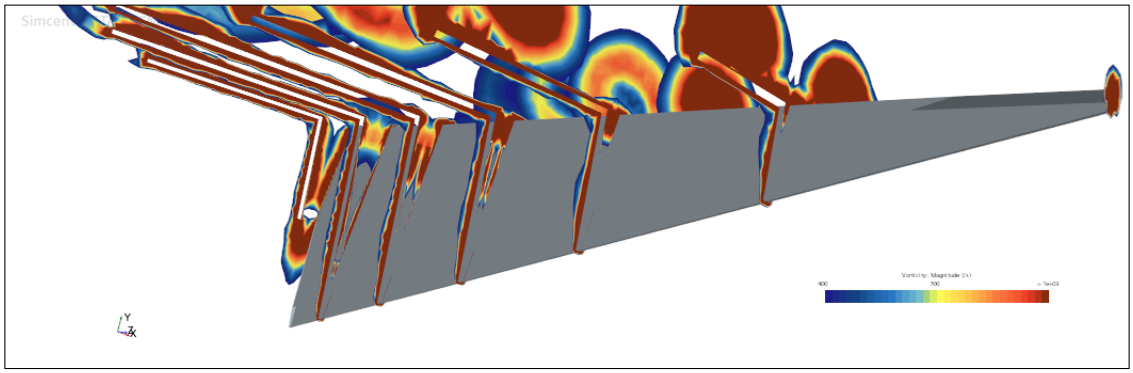

Fig. 16 Contours of vorticity at $\alpha = 30°$

To understand which distance, downstream from leading edge of the ventral gap is effective, vorticity vector contours are visualized on a plane along the length of the ventral gap. The Fig.17 shows the vorticity vector +i (+x direction) and +j (+z direction) respectively. The reader must note that the free-stream flow direction is in -z direction and +x is pointing out-of the page. The scale of the vorticity map is (-400,400) m/s. This way of depicting the contours comes from the fact that the vorticity is curl of velocity and -ve vorticity means the flow rotates clockwise relative to chosen frame of reference. Because the visualization is on a plane, -ve vorticity means the flow is moving locally in direction of reference vector. For better understanding of the contours, as a rule of thumb, in the areas where it is blue (-ve vorticity) the local vorticity vector is pointing towards +x (in Fig.17(a)) and +z (in Fig.17(b)), which means locally the flow is moving in that direction. In the areas of yellow and red (+ve vorticity) the local vector is in opposite direction.

Four positions along the length of the ventral gap were identified where interesting phenomenon can be seen. From the nose to position 1 the flow is more influenced by the main vortex that forms at the LE of the wing, which is seen previously. The gap is also not big enough for the flow to enter the cavity and follow it.

From position 1-2, the flow is into the cavity and following the ventral gap. There is also a slight hint of formation of vortex at the bottom of the gap. At the end these small vortex is not doing much and mixing with the flow. This is because of strong entrainment effect happening downstream the position 2. This is because of the fact that the main vortex core on the wings is moving inwards because of change in sweep angle. This might be influencing the flow in ventral gap to raise and move span-wise towards the vortex.

Between 2-3, It can be seen that the flow experience a strong vorticity. As a matter of fact, as we move downstream the ventral gap is widening and this provide a spacial condition for the flow to turn into the ventral gap, which gives an idea of formation of induced vortex. At position 3 and downstream, a down-wash flow exists after the vorticity because of the entrainment effect and widening of the ventral gap. Between the vorticity and down-wash flow there lies a dead-flow area (between 3-4). This area acts as a comparatively high-pressure zone near the trailing edge, which can be seen in Fig.18(b) (black circle) as well, which is obviously not present in the ventral gap-closed configuration.

At the trailing edge (position 4), this back-flow induced vortex formed in the top part of the ventral gap seems to be sustained by feeding the incoming cavity flow. In the bottom region of the gap, below this vortex, the down-wash flow produces another back-flow after encountering the high-pressure area at the trailing-edge.

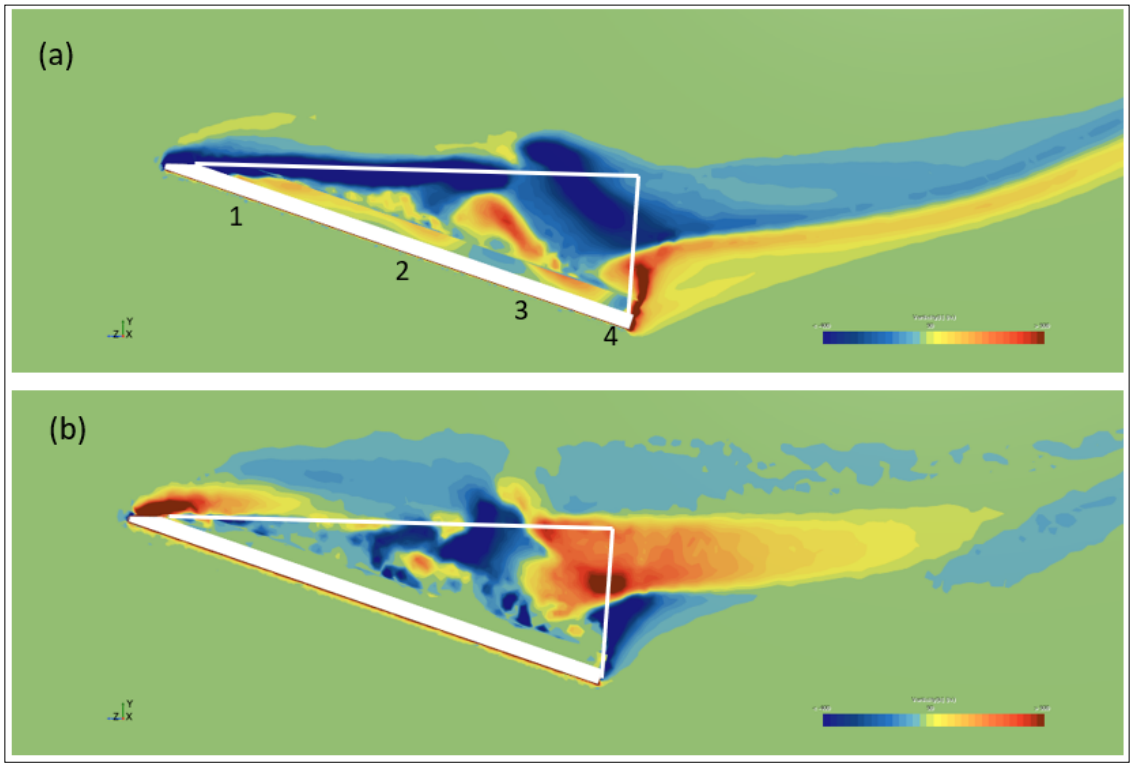

Fig. 17 Contours of vorticity vector in (a)+x direction and (b)+z direction at $\alpha = 30°$. The white lines represents the boarder of the ventral-gap.

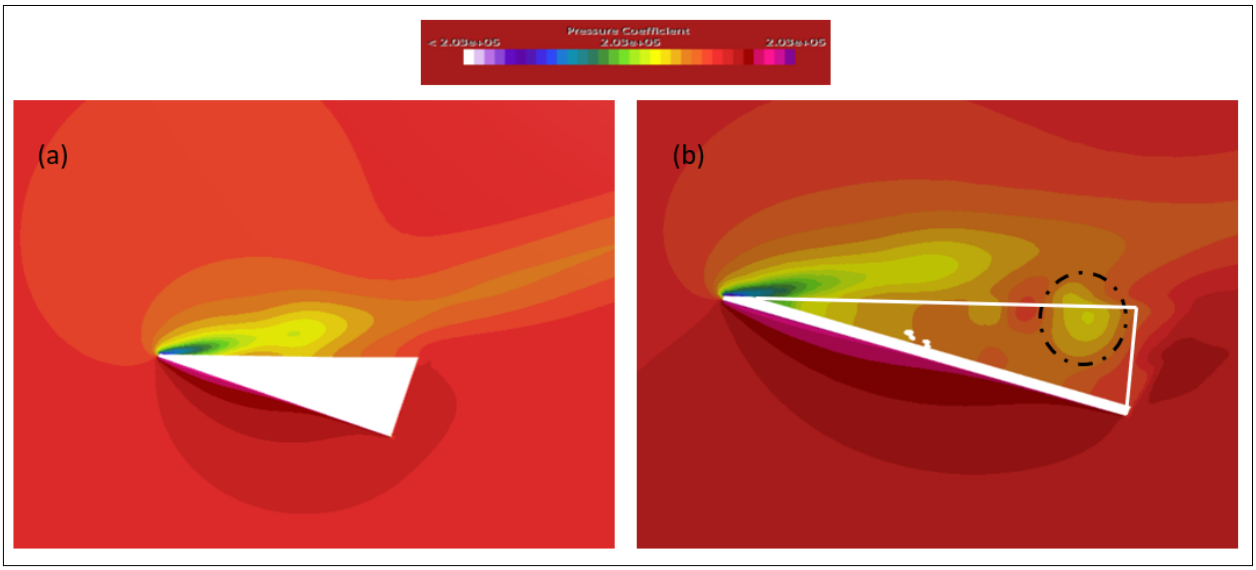

Fig. 18 Contours of pressure coefficient (absolute) along the chord. (a)Ventral-closed, (b)Ventral-opened configurations at $\alpha = 30°$

The Fig.19 shows the airflow velocity distribution of the two configurations at z/c = 0.89 and it can be seen that the velocity distribution at the ventral gap of the ventral gap-opened configuration agrees well with the backflow vortex. At the vortex core the flow speed decline to about 0, which is shown in the blue area within the ventral gap in Fig.19(b).

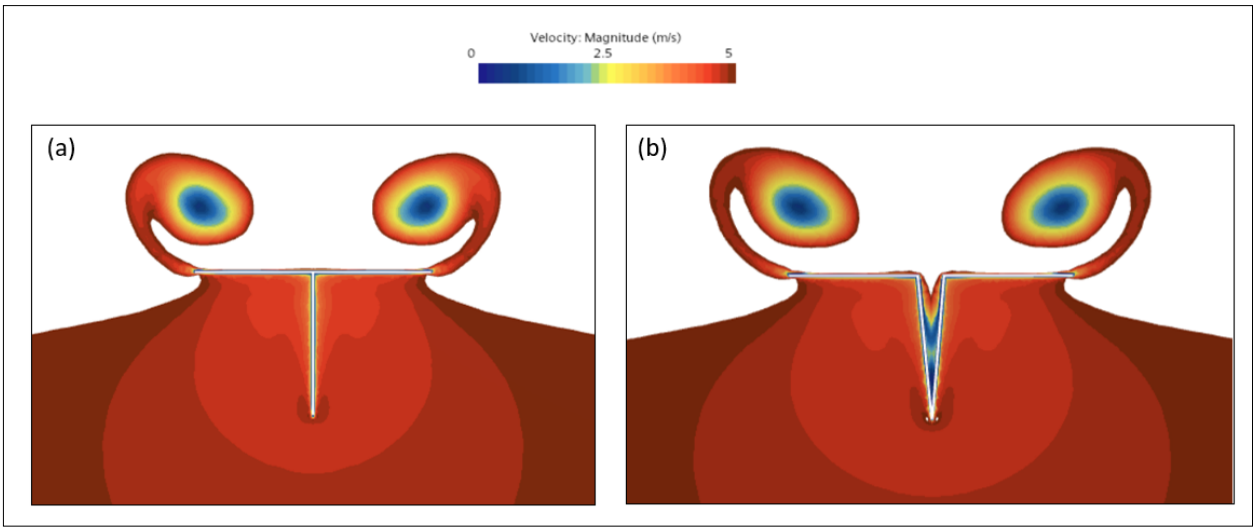

Fig. 19 Contours of velocity at z/c = 0.89 (a)Ventral-closed, (b)Ventral-opened configurations at $\alpha = 30°$

VII. Analysis of the Pressure distribution

The influence of these phenomenon on pressure distribution along the span of the paper-plane with clip planes at different z/c will be discussed next to understand the additional lift in case of ventral-opened configuration.

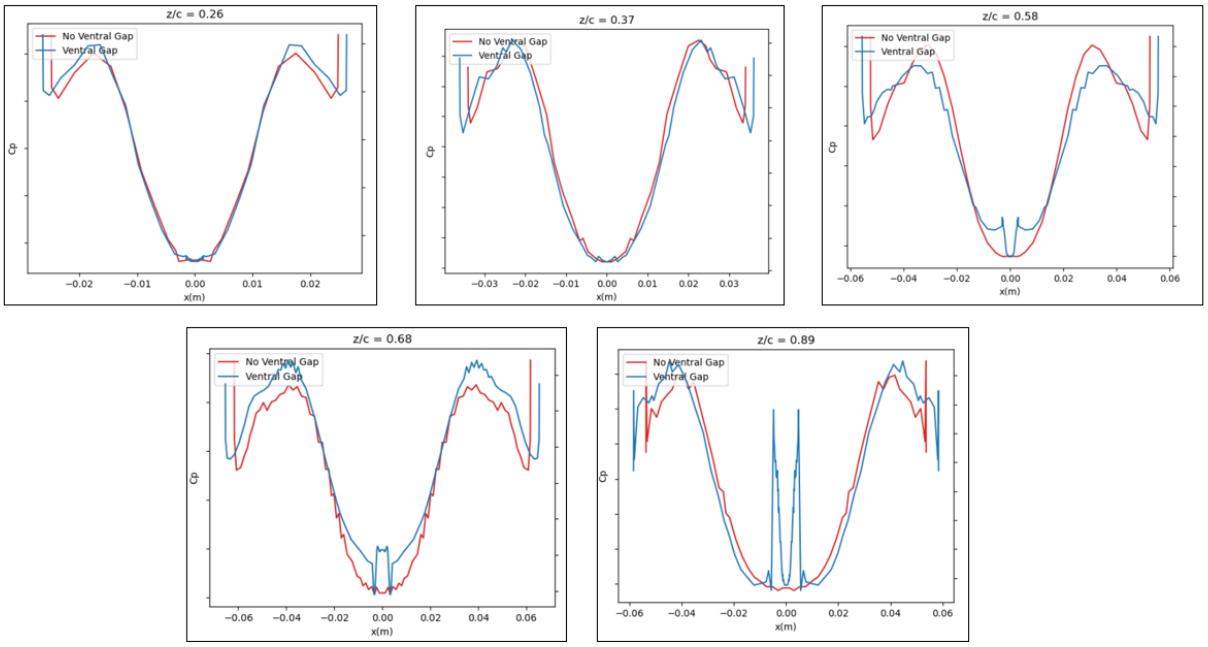

;

Fig. 20 Variation of CP in span, on upper surface of the plane with clip position at z/c - 0.26, 0.37, 0.58, 0.68 and 0.89 respectively at $\alpha = 30°$.

The characteristics discussed in previous section are reflected in the Fig.20. For example, the configuration with ventral gap opened has higher low-pressure zone over the inner part at z/c = 0.58 which is approximately at position 2 mentioned before. Downstream at z/c = 0.68 this is notably evident which indicates formation of induced vortex. At the trailing edge, z/c = 0.89, peaks can be seen in the center which indicated the presence of back-flow vortex. One more point to note is that, for example at z/c=0.68 has strong low-pressure zones over the outer part and position of this main vortex is slightly more outwards compared to no ventral configuration.

The displacement and strengthening of the vortex due to the secondary flow, along with the creation of an induced vortex at the center, may contribute to the lift enhancement. Tests on a delta wing employing lateral blowing to regulate the wing vortex intensity demonstrated that this blowing method enhances the vortex and raises lift. The extra flow generated by the ventral gap replicates the blowing effect seen in Celik and Roberts' [1] experiments. Despite the weaker secondary flow in this study relative to the blowing rates in the experiments, the outcomes suggest that it effectively modifies the wing vortex and enhances lift.

VIII. Design of the Dart

From the flow analysis done, the conclusion is drawn that the ventral gap near the nose of the paper-plane has no effect on the flow enhancement compared to the no ventral gap configuration. Hence, folding technique can be changed to have extra part of paper to wrap around and cover this gap. An added benefit is that this warping fold can act as locking fold and hold the paper-plane without opening up during high-velocity throws. (See Fig.21). The center part and ventral gap at trailing edge are helpful to benefit from extra lift because of the flow entrainment and induced vortex.

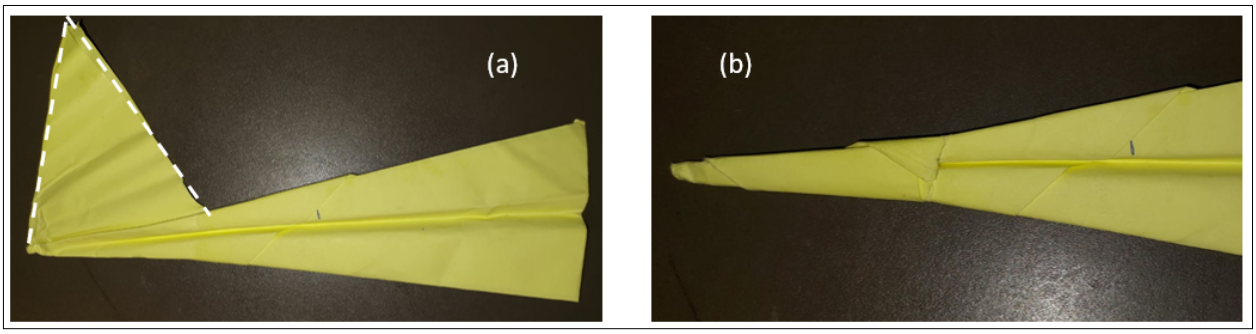

Fig. 21 The Warping fold step of the Dart design.

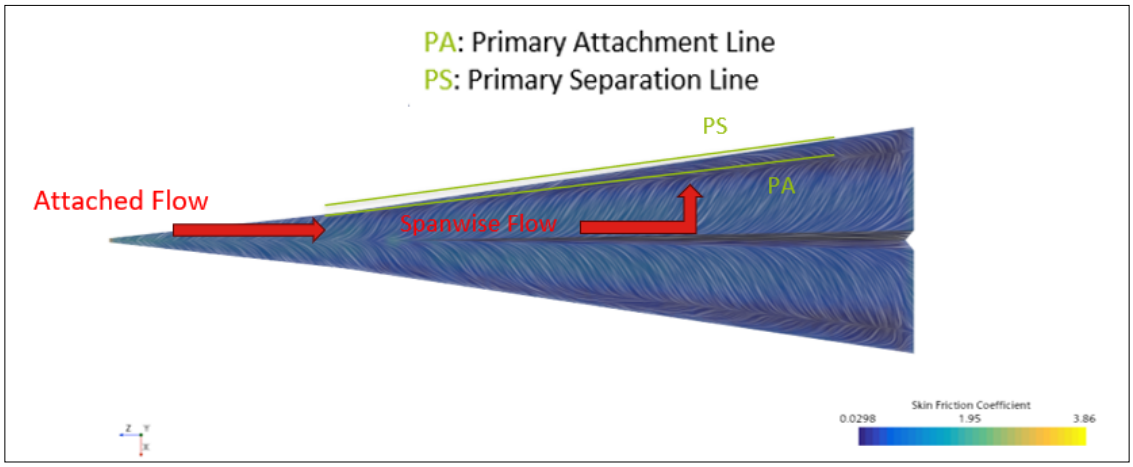

Fig. 22 Skin friction coefficient on upper surface Dart design at $\alpha = 30°$.

Computational study was performed and flow analysis is done on the dart model to see if the idea behind the design still holds true. The Fig.22 shows the skin-friction coefficient on the upper surface of the model. The flow is attached at the nose and the main vortex forms at the LE because of spanwise flow due to sweep. Both, the primary separation line and primary attachment line can be seen. In the vicinity of the ventral gap there are no notable secondary flow effects as seen previously in the Suzanne ventral-gap opened configuration.

The reason can be the size of this ventral gap, which is smaller compared to the Suzanne's case. The gap is not big enough for the flow to enter into the gap and develop as ventral-gap-flow. So the flow is more influenced by the main vortex and the incoming flow.

IX. Conclusion

Flow analysis is conducted to better understand the reason for the performance of Suzanne (former World Record holder) and the effect of the ventral gap on the performance is analyzed through flow analysis. The model with the ventral gap open performed better with higher lift, but there are practical disadvantages of not holding the shape during testing and also its stall angle is lower when compared to closed gap configuration.

The main conclusions drawn from the comparative analysis of ventral gap opened and closed configurations, are:

- The ventral gap at the nose has no major influence on the flow and the incoming flow is influenced more by the main vortex that are formed at the LE.
- Downstream, the central part of the ventral gap is where interesting phenomena like flow entrainment of the flow following the ventral gap and formation of induced vortex are observed.

- At the aft(trailing edge), the back-flow induced vortex is formed at the top region of the gap and in the lower region, below this vortex, the down-wash flow produces another back-flow after encountering area of high pressure at the trailing-edge.

With these conclusions, a dart plane with a partial ventral gap is folded and tested. The flow over the dart is same as it would be in-case of slender delta-wing, and the height of the ventral gap is not large enough for the flow to develop as assumed during the design phase. To better understand the influence on the ventral-gap, a study is required to understand the influence of different parameters like the height and angle of the ventral-gap. Which is not performed during this present study.

Though the C_l is less for the dart model, the C_l/C_d is an important parameter to understand the performance. Though it is approximately similar for all models at higher AOA, lower drag and compactness of the dart allowed to get a average maximum range of 30m during flight test.

References

[1] Zeli Celik and Leonard Roberts. "Vortical flow control on a delta wing by lateral blowing". In: *32nd Aerospace Sciences Meeting and Exhibit*. American Institute of Aeronautics and Astronautics. Jan. 1994. DOI: 10.2514/6.1994-509. URL: https://doi.org/10.2514/6.1994-509.

[2] Min Chang et al. "Flow analysis on the ventral gap of a paper airplane". In: *J Mechanical Engineering Science* (July 2020).

[3] John Collins. *The Paper Airplane Guy*. Accessed: 2024-02-01. 2024. URL: https://www.thepaperairplaneguy.com/.

[4] James Luckring. "The discovery and prediction of vortex flow aerodynamics". In: *The Aeronautical Journal* 123 (June 2019), pp. 729–804. DOI: 10.1017/aer.2019.43.

[5] Edward C Polhamus. "A concept of the vortex lift of sharp-edge delta wings based on a leading-edge-suction analogy". In: *Aeronautical Journal* (1966).

[6] Jorg Schluter. "Aerodynamic study of the dart paper airplane for micro air vehicle application". In: *Proceedings of the Institution of Mechanical Engineers, Part G: Journal of Aerospace Engineering* 228 (Feb. 2013), pp. 567–576. DOI: 10.1177/0954410013476778.